TRAVELLING-WAVE SIMILARITY SOLUTION FOR UNSTEADY FLOW AROUND A DRY PATCH DRIVEN BY GRAVITY AND CONSTANT SURFACE SHEAR STRESS

Yazariah M. Yatim
School of Mathematical Sciences
Universiti Sains Malaysia
11800 USM
Penang, Malaysia
Email: yazariahmy@usm.my
Web page: www.mat.usm.my/math/

Brian R. Duffy and Stephen K. Wilson
Department of Mathematics and Statistics
University of Strathclyde
Livingstone Tower, 26 Richmond Street
Glasgow G1 1XH, UK
Email: b.r.duffy@strath.ac.uk
Web page: www.mathstat.strath.ac.uk/

Abstract

In this paper we use the lubrication approximation to analyse three-dimensional unsteady flow of a thin film of Newtonian fluid around a symmetric slender moving dry patch on an inclined planar substrate. The flow being driven by gravity and a prescribed constant shear stress at the free surface. We obtain a novel unsteady travelling-wave similarity solution for the dry patch of uniform thickness, in which the dry patch travels at constant speed. This solution predicts that the dry patch has a parabolic shape which may be concave up or concave down the substrate. In all cases investigated numerically the film thickness is found to increase monotonically away from the contact line.

Key words: travelling-wave similarity solution, dry patch, Newtonian fluid, thin-film flow.

1 INTRODUCTION

Dry patches can occur in both stationary and flowing fluid films for a variety of reasons, including dry-out due to localised heating, the presence of air bubbles within the film, inhomogeneities of the substrate, and the presence of surfactants. There is particular interest in dry patches in films that arise in industrial contexts, such as coating processes and heat exchangers; in particular, in coating processes, uncoated regions of the substrate may seriously degrade the quality of the final product. As a consequence, the formation, stability and evolution of dry patches in fluid films are problems of enduring theoretical, experimental and practical interest.

Pioneering work on a dry patch in a flowing fluid film driven either by gravity or by a prescribed surface shear stress due to an external air flow was performed by [2] and extended by [9]. Two steady similarity solutions for a flow around a non-uniform slender dry patch in a thin film draining under gravity on an inclined plane, namely one for the case of weak surface tension and one for the case of strong surface tension were obtained

by [6]. Early experiments on the shape and structure of a dry patch in a fluid film draining under gravity down the outside of a vertical circular cylinder were performed by [1], and over the last decade or so the shape and structure of a dry patch in a fluid film draining under gravity down an inclined plane has been extensively studied both experimentally and theoretically by Limat and his collaborators ([7], [8], [3], [4], and [5]).

In the present paper we generalise the problem of slender dry patch in a thin fluid film driven purely by gravity studied by [10] to the problem of slender dry patch in a fluid film driven by gravity and a prescribed constant surface shear stress.

2 PROBLEM FORMULATION

Consider a thin film of Newtonian fluid with constant density ρ and constant viscosity μ on a planar substrate inclined at an angle α $(0 < \alpha < \pi)$ to the horizontal, subject to gravitational acceleration g and a prescribed constant shear stress τ on its free surface acting up or down the slope. We shall be concerned with unsteady flow of such a film around a dry patch on the substrate, as sketched in Figure 1.

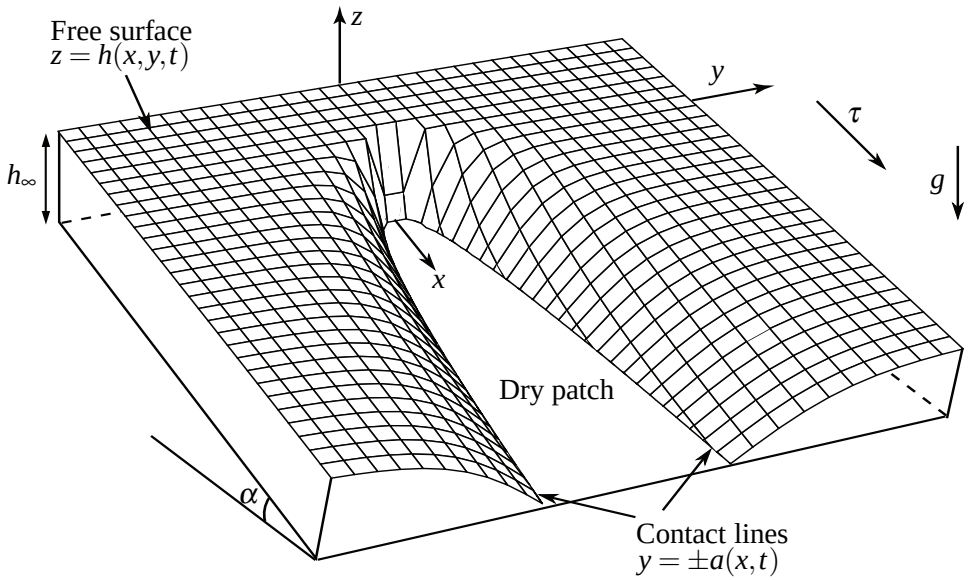

Figure 1: Sketch of the geometry of the problem: a moving dry patch in a thin film.

When $0 < \alpha < \pi/2$ the fluid is on the upper side of the substrate, representing the sessile case, and when $\pi/2 < \alpha < \pi$ it is on the underside of the substrate, representing the pendent case. Cartesian axes $Oxyz$ with the x axis down the line of greatest slope and the z axis normal to the substrate are adopted, with the substrate at $z = 0$; the free surface profile of the film is denoted by $z = h(x,y,t)$, where t denotes time. The prescribed surface shear stress acts down the substrate if $\tau > 0$, and acts up if $\tau < 0$.

We take the dry patch to be slender (varying much more slowly in the longitudinal (x) direction than in the transverse (y) direction), and we neglect surface-tension effects. Then with the familiar lubrication approximation, the velocity (u,v,w), pressure p and thickness h satisfy the governing equations

$$u_x + v_y + w_z = 0, \tag{1}$$

$$\mu u_{zz} + \rho g \sin\alpha = 0, \tag{2}$$

$$-p_y+\mu v_{zz}=0, \tag{3}$$

$$-p_z-\rho g\cos\alpha=0, \tag{4}$$

subject to the boundary conditions of no slip and no penetration on the substrate $z=0$:

$$u=0, \quad v=w=0, \tag{5}$$

balances of normal and tangential stresses on the free surface $z=h$:

$$p=p_{\rm a}, \quad \mu u_z=\tau, \quad v_z=0 \tag{6}$$

(where $p_{\rm a}$ denotes atmospheric pressure), and the kinematic condition on $z=h$:

$$h_t+\bar{u}_x+\bar{v}_y=0, \tag{7}$$

where the local fluxes $\bar{u}=\bar{u}(x,y,t)$ and $\bar{v}=\bar{v}(x,y,t)$ are defined by

$$\bar{u}=\int_0^h u\,{\rm d}z, \quad \bar{v}=\int_0^h v\,{\rm d}z. \tag{8}$$

Integration of (1)–(4) subject to (5) at $z=0$ and (6) at $z=h$ yields

$$p=p_{\rm a}+\rho g\cos\alpha\,(h-z)\,, \tag{9}$$

$$u=\frac{\rho g\sin\alpha}{2\mu}\,(2h-z)\,z+\frac{\tau}{\mu}z, \tag{10}$$

$$v=-\frac{\rho g\cos\alpha}{2\mu}h_y\,(2h-z)\,z, \tag{11}$$

$$w=\frac{\rho g\cos\alpha}{2\mu}\left(hh_{yy}+h_y^2-\frac{h_{yy}z}{3}\right)z^2-\frac{\rho g\sin\alpha}{2\mu}h_x z^2. \tag{12}$$

Substituting (10) and (11) into (8) gives

$$\bar{u}=\frac{\rho g\sin\alpha}{3\mu}h^3+\frac{\tau}{2\mu}h^2, \quad \bar{v}=-\frac{\rho g\cos\alpha}{3\mu}h^3h_y, \tag{13}$$

and hence the kinematic condition (7) yields the governing partial differential equation for h:

$$h_t=\frac{\rho g\cos\alpha}{3\mu}\left(h^3h_y\right)_y-\frac{\rho g\sin\alpha}{3\mu}\left(h^3\right)_x-\frac{\tau}{2\mu}\left(h^2\right)_x. \tag{14}$$

Once h is determined from (14) the solution for p, u, v and w in (9)–(12) is known.

In the case of a film of constant uniform thickness h_∞ the solution takes the form $p=p_\infty=p_\infty(z)$, $u=u_\infty=u_\infty(z)$, $v=v_\infty=0$ and $w=w_\infty=0$, where

$$p_\infty=p_{\rm a}+\rho g\cos\alpha\,(h_\infty-z)\,, \quad u_\infty=\frac{\rho g\sin\alpha}{2\mu}\,(2h_\infty-z)\,z+\frac{\tau}{\mu}z, \tag{15}$$

representing steady unidirectional flow up or down the substrate, with depth-averaged velocity $U_\infty\mathbf{i}$, where

$$U_\infty=\frac{\rho g\sin\alpha}{3\mu}h_\infty^2+\frac{\tau}{2\mu}h_\infty, \tag{16}$$

which may be positive, negative or zero. For later use we note that the shear stress $\tau_\infty = \mu \mathrm{d}u_\infty/\mathrm{d}z$ at $z = 0$ acting on the substrate due to this flow is given by

$$\tau_\infty = \rho g \sin\alpha h_\infty + \tau, \tag{17}$$

which also may be positive, negative or zero.

We are concerned with unsteady flow around a dry patch in a film of thickness h_∞ at infinity (that is, in a film that would be of uniform thickness h_∞ if the dry patch were absent). We shall restrict attention to dry patches that are symmetric about $y = 0$ (so that h is even in y) with (unknown) semi-width $a = a(x,t)$, so that the fluid occupies $|y| \geq a$, and $h = 0$ at the contact lines $y = \pm a$. From (13) we have $\bar{u} = 0$ at $y = \pm a$, so that the zero-mass-flux condition at the contact lines, namely

$$\bar{v} = \pm a_x \bar{u} \quad \text{at} \quad y = \pm a, \tag{18}$$

reduces to $\bar{v} = 0$ at $y = \pm a$, and therefore we have the contact-line conditions

$$h = 0 \quad \text{at} \quad y = \pm a, \qquad h^3 h_y \to 0 \quad \text{as} \quad y \to \pm a. \tag{19}$$

2.1 A travelling-wave similarity solution

We seek an unsteady travelling-wave similarity solution of (14) in the form

$$\left.\begin{array}{ll} h = h_\infty F(\eta), \quad \eta = \dfrac{y}{[\ell(x-ct)]^n} & \text{if } \ell(x-ct) \geq 0, \\ h = h_\infty & \text{if } \ell(x-ct) < 0, \end{array}\right\} \tag{20}$$

where $c\mathbf{i}$ (with c positive, negative or zero) is the velocity of the dry patch up or down the substrate, the constant ℓ ($\neq 0$) is to be specified, and the exponent n and the dimensionless function $F = F(\eta)$ (≥ 0) of the dimensionless similarity variable η are to be determined. The dry patch lies in the region where $\ell(x-ct) \geq 0$, and the fluid in the region where $\ell(x-ct) < 0$ (ahead of or behind the dry patch) is of uniform thickness h_∞; at $x = ct$ the thickness h and its derivative h_y are continuous (so that u, v and p are continuous there), except at the singular point $x = ct$, $y = 0$, at which the free surface is normal to the substrate, occupying $0 \leq z \leq h_\infty$.

With $(20)_1$ the terms in (14) balance provided that $n = 1/2$ (so that ℓ has physical dimensions of length), and then (14) reduces to an ordinary differential equation for $F(\eta)$, namely

$$4\rho g \cos\alpha h_\infty^3 \left(F^3 F'\right)' + \ell\eta \left[2\rho g \sin\alpha h_\infty^2 F^3 + 3\tau h_\infty F^2 - 6\mu c F\right]' = 0, \tag{21}$$

where a dash denotes differentiation with respect to η.

We denote the (unknown) position where $F = 0$ by $\eta = \eta_0$ (corresponding to the contact-line position $y = a$), so that the fluid lies in $|\eta| \geq \eta_0$, and

$$a = \sqrt{\ell(x-ct)}\,\eta_0, \quad \frac{y}{a} = \frac{\eta}{\eta_0}, \tag{22}$$

showing that the dry patch has a parabolic shape. From (19) we have

$$F = 0 \quad \text{at} \quad \eta = \eta_0, \qquad F^3 F' \to 0 \quad \text{as} \quad \eta \to \eta_0; \tag{23}$$

in addition, F must satisfy the far-field condition

$$F \to 1 \quad \text{as} \quad \eta \to \infty. \tag{24}$$

As we shall see, the value of η_0 is not determined as part of the solution, in general, so that (20) represents a family of possible solutions.

If F were to have any stationary points in $\eta \geq \eta_0$ then equation (21) would require all derivatives of F to be zero there, indicating that, in fact, F has no stationary points, and so increases monotonically with η from $F = 0$ at $\eta = \eta_0$ to $F \to 1$ as $\eta \to \infty$; this is consistent with numerical results presented later.

With $(20)_1$ the level sets of h are the curves $\eta =$ constant, that is, the film thickness is the same at all points (x,y) on each of the parabolae $y^2 \propto \ell(x-ct)$ (≥ 0).

2.2 Behaviour near $\eta = \eta_0$

Near the contact line $\eta = \eta_0$ it is found from (21) that

$$F \sim \left[\frac{9\eta_0\mu\ell c(\eta-\eta_0)}{2\rho g\cos\alpha h_\infty^3}\right]^{\frac{1}{3}} \tag{25}$$

as $\eta \to \eta_0^+$, which can be valid only if

$$\ell\cos\alpha c > 0. \tag{26}$$

Equation (25) shows that the fluid film has infinite slope at the contact line $\eta = \eta_0$, and so the lubrication approximation fails there, and there is no freedom to impose prescribed conditions on the three-phase contact angle.

2.3 Behaviour in the limit $\eta \to \infty$

In the limit $\eta \to \infty$ we write $F = 1 + f$ with $|f| \ll 1$ in (21), in which case $f = f(\eta)$ satisfies

$$f'' + K\eta f' = 0, \tag{27}$$

where we have defined the constant K by

$$K = \frac{3\ell}{2\rho g\cos\alpha h_\infty^2}\left(\tau_\infty - \frac{\mu}{h_\infty}c\right). \tag{28}$$

Equation (27) has a solution for f satisfying $f \to 0$ as $\eta \to \infty$ only if $K > 0$, and in that case F has the far-field behaviour

$$F - 1 \propto \frac{1}{\eta}\exp\left(-\frac{K\eta^2}{2}\right) \tag{29}$$

as $\eta \to \infty$, showing that the transverse profile of the fluid film approaches the uniform far-field value in (24) monotonically.

2.4 Physical forms of the solutions

The condition $K > 0$ together with condition (26) shows that a dry patch is possible only if

$$\ell \cos\alpha h_\infty \tau_\infty > \mu \ell \cos\alpha c > 0. \tag{30}$$

Thus in the sessile case ($\cos\alpha > 0$) if $\tau_\infty > 0$ then $\ell > 0$ and $c > 0$, so that the dry patch occupies $x \geq ct$, moves *downwards* relative to the substrate, and has semi-width $a = \sqrt{\ell(x-ct)}\,\eta_0$, widening with increasing x, the fluid in $x < ct$ being of uniform thickness h_∞, whereas if $\tau_\infty < 0$ then $\ell < 0$ and $c < 0$, so that the dry patch occupies $x \leq ct$, moves *upwards* relative to the substrate, and has semi-width $a = \sqrt{|\ell|(ct-x)}\,\eta_0$, narrowing with increasing x, the fluid in $x > ct$ being of uniform thickness h_∞; analogous remarks apply to the pendent case ($\cos\alpha < 0$).

2.5 Non-dimensionalisation

We are now in a position to choose ℓ and non-dimensionalise variables. Since U_∞ in (16) could be zero, it is not convenient to use it as a velocity scale, so instead we choose to non-dimensionalise velocities in the x direction using a velocity scale U associated with purely gravity-driven flow, namely $U = \rho g \sin\alpha h_\infty^2/\mu$; correspondingly we non-dimensionalise shear stresses with the stress scale $T = \rho g \sin\alpha h_\infty$. Thus we non-dimensionalise and re-scale variables according to

$$\begin{gathered} x = Xx^*, \quad y = \sqrt{|\ell|X}y^*, \quad z = h_\infty z^*, \quad t = \frac{X}{U}t^*, \quad h = h_\infty h^*, \quad a = \sqrt{|\ell|X}a^*, \\ u = Uu^*, \quad v = \sqrt{\frac{|\ell|}{X}}Uv^*, \quad w = \frac{Uh_\infty}{X}w^*, \quad c = Uc^*, \quad U_\infty = UU_\infty^*, \\ p = p_\mathrm{a} + \rho g|\cos\alpha|h_\infty p^*, \quad \tau = T\tau^*, \quad \tau_\infty = T\tau_\infty^*, \end{gathered} \tag{31}$$

where X ($\gg h_\infty$) is a length scale in the x direction, which we may choose arbitrarily. Also, consistent with (30), and without loss of generality, we now write ℓ in the form

$$\ell = S_\infty S_g h_\infty |\cot\alpha|, \tag{32}$$

where we have introduced the notation $S_g = \mathrm{sgn}(\cos\alpha) = \pm 1$ and $S_\infty = \mathrm{sgn}(\tau_\infty) = \pm 1$, with now $\tau_\infty = 1 + \tau$; then (30) reduces to $|\tau_\infty| > S_\infty c > 0$, that is,

$$0 < c < \tau_\infty \quad \text{or} \quad \tau_\infty < c < 0. \tag{33}$$

Conditions for the fluid film to be thin and the dry patch to be slender are that the length scales in the x, y and z directions, namely X, $\sqrt{|\ell|X}$ and h_∞, satisfy $h_\infty \ll \sqrt{|\ell|X} \ll X$, so that

$$X \gg h_\infty |\cot\alpha|, \quad X \gg h_\infty |\tan\alpha|, \tag{34}$$

showing that X must be much larger than h_∞ and that α cannot be close to 0, $\pi/2$ or π.

With stars on non-dimensional variables dropped for clarity the solution (20) takes the slightly simpler form

$$\left.\begin{aligned} &h = F(\eta), \quad \eta = \frac{y}{\sqrt{S_\infty S_g\,(x-ct)}} && \text{if } S_\infty S_g(x-ct) \geq 0, \\ &h = 1 && \text{if } S_\infty S_g(x-ct) < 0, \end{aligned}\right\} \tag{35}$$

and

$$a = \sqrt{S_\infty S_g\,(x-ct)}\,\eta_0, \tag{36}$$

with F satisfying

$$4\left(F^3F'\right)' + S_\infty\eta\left[2F^3 + 3\tau F^2 - 6cF\right]' = 0, \tag{37}$$

to be integrated subject to (23) and (24). Near the contact line $\eta = \eta_0$ equation (25) gives

$$F \sim \left[\frac{9}{2}\eta_0 S_\infty c(\eta-\eta_0)\right]^{\frac{1}{3}} \tag{38}$$

if $c \neq 0$; also F again has the far-field behaviour (29) with now $K = 3S_\infty(\tau_\infty - c)/2$ (> 0).

2.6 Numerical solution

A closed-form solution of (37) for F is not available, and so we solved it numerically, using a shooting method, by shooting from a chosen value of the contact-line position $\eta = \eta_0$, with chosen values of τ and c. The solution F was monitored to see if it satisfied an approximated version of (24), namely

$$F = 1 \quad \text{at} \quad \eta = \eta_\infty\ (\gg \eta_0), \tag{39}$$

to within a prescribed tolerance; if not then the value of c was changed and the calculation repeated until a solution satisfying (39) for the chosen values of η_0 and τ was found. In fact, the numerical computation cannot be started at $\eta = \eta_0$ (because of the singular slope there, given by (38)), so instead it was started from a position $\eta = \eta_0 + \delta$, where δ (> 0) is small; thus we solved (37) subject to the approximated boundary conditions

$$F(\eta_0+\delta) = \left[\frac{9\eta_0 S_\infty c\delta}{2}\right]^{\frac{1}{3}}, \quad F'(\eta_0+\delta) = \left[\frac{\eta_0 S_\infty c}{6\delta^2}\right]^{\frac{1}{3}}, \tag{40}$$

obtained from (38). This procedure was then repeated with smaller values of δ (as small as $\delta = 10^{-10}$) and larger values of η_∞ (as large as $\eta_\infty = 10^3$) until the solution converged to within a prescribed tolerance.

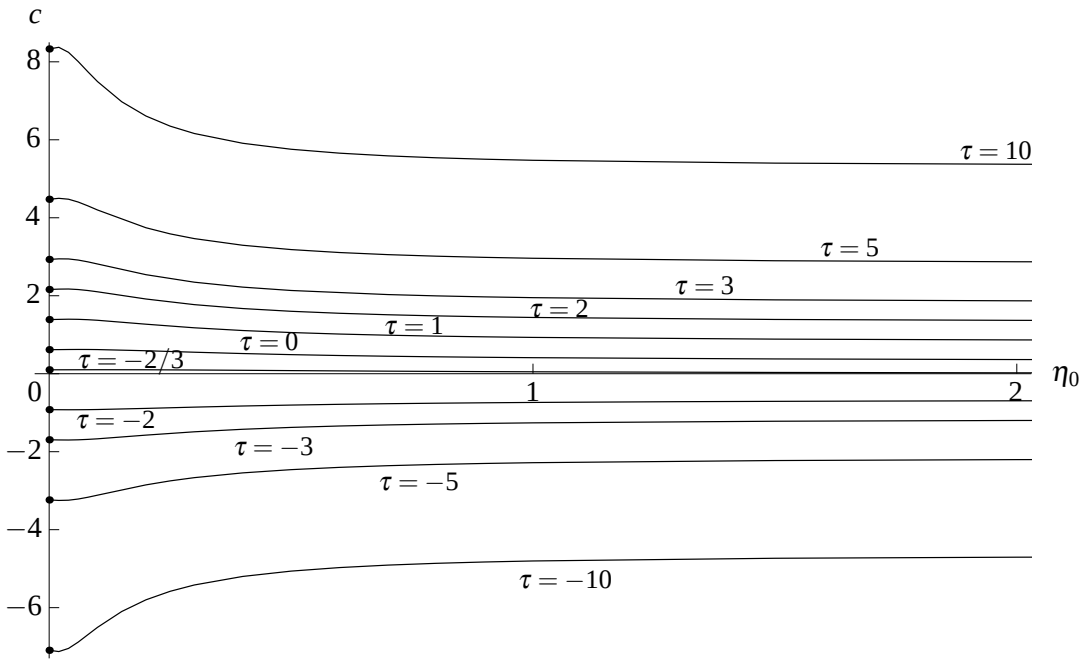

Figure 2: Plot of c as a function of η_0 for various τ.

Figure 2 shows plots of solution curves for c as a function of η_0 obtained by the above procedure, for a range of values of τ. Figure 3 shows an enlargement of Figure 2, giving additional solution curves near the η_0 axis, and Figures 4 and 5 show enlargement of Figure 3.

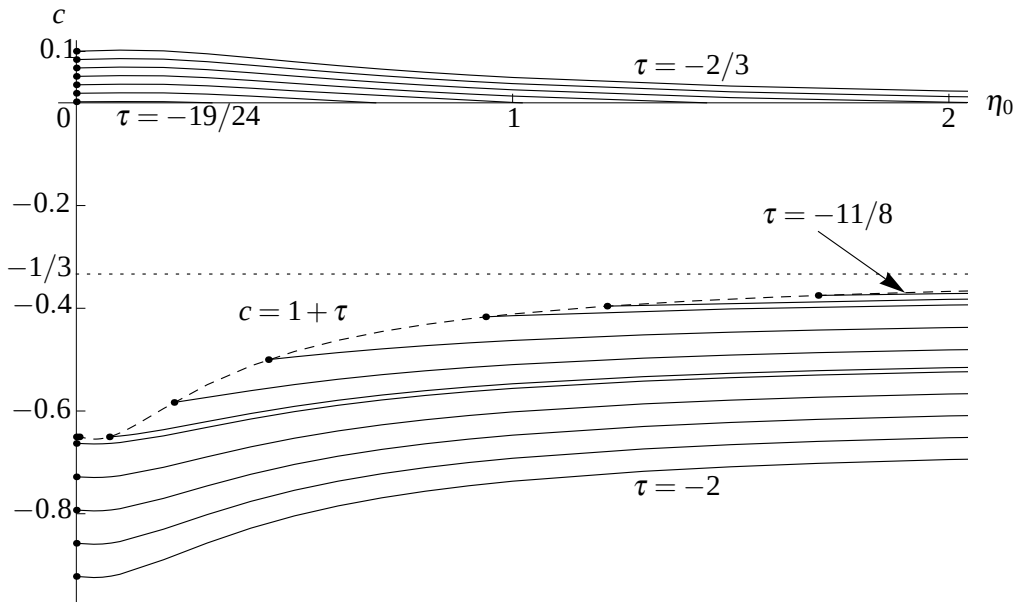

Figure 3: Enlargement of Figure 2, showing c as a function of η_0 for $\tau = -2/3$, $-11/16$, $-17/24$, $-35/48$, $-3/4$, $-37/48$, $-19/24$ (upper group) and $\tau = -11/8$, $-67/48$, $-17/12$, $-3/2$, $-19/12$, τ_{c4} ($\simeq -1.6504$), $-5/3$, $-7/4$, $-11/6$, $-23/12$, -2 (lower group). The *bounding curve* on which $c = 1+\tau$ is shown dashed, and the asymptote of this curve at large η_0, namely $c = -1/3$, is shown dotted; there is no solution in the region between this bounding curve and the η_0 axis.

Some of the information in Figures 2–5 can be summarised as follows. There can be a solution c (and hence the similarity solution (20) is valid) if either $\tau \geq \tau_{c1} \simeq -0.7947$ (in which case $c \geq 0$) or $\tau < -4/3$ (in which case $c < 0$), but there is no solution for $-4/3 \leq \tau < \tau_{c1}$; for $\tau = \tau_{c1}$ there is a single solution $c = 0$, for which $\eta_0 \simeq 0.1386$. For $\tau \geq -2/3$ and for $\tau \leq \tau_{c3} \simeq -1.6547$ there is a solution c for any value of η_0. For $\tau_{c1} \leq \tau < -2/3$ there is a solution c only for a finite interval of η_0 values, and for $\tau_{c3} < \tau < -4/3$ there is a solution c for sufficiently large η_0, as well as for an additional finite interval of η_0 values for some τ; in all these cases the η_0 intervals in which solutions exist depend on the value of τ. The curve for $\tau = \tau_{c2} \simeq -0.7941$ is the one that passes through $\eta = 0$, $c = 0$. In Figures 3 and 5 the *bounding curve* arising from $(33)_2$, namely $c = 1+\tau$ (< 0) (on which $c \to -1/3$ as $\eta_0 \to \infty$), is shown dashed; by $(33)_2$ any solution curve intersecting this bounding curve cannot lie below the point of intersection. The solution curve for $\tau = \tau_{c3}$ is the one that pass through the minimum on the bounding curve, the (discontinuous) solution curve for $\tau = \tau_{c4} \simeq -1.6504$ is the one that intersects the bounding curve at $\eta_0 = 0$, and the (discontinuous) solution curve for $\tau = \tau_{c5} \simeq -1.6502$ is the one that just touches the bounding curve at its maximum.

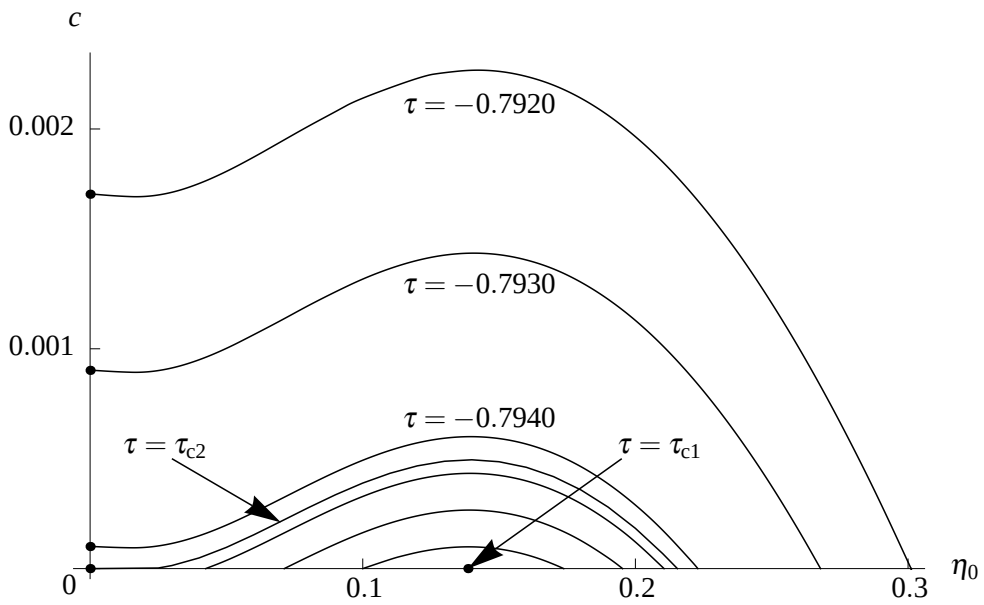

Figure 4: Enlargement of Figure 3, showing c as a function of η_0 for $\tau = -0.792$, -0.793, -0.794, τ_{c2} ($\simeq -0.7941$),-0.7942, -0.7944, -0.7946 and τ_{c1} ($\simeq -0.7947$).

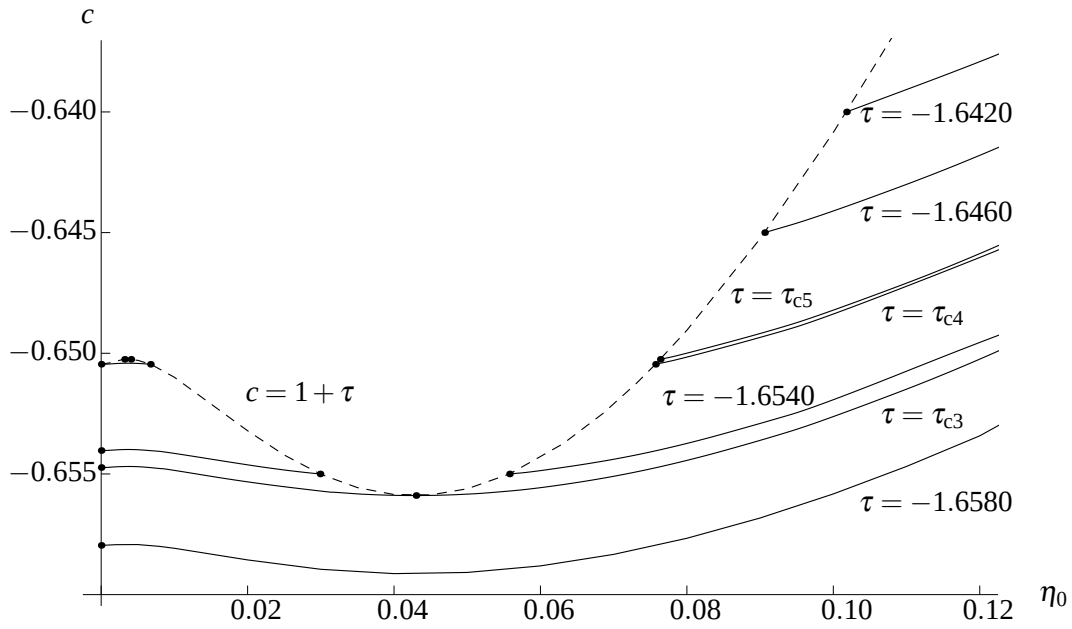

Figure 5: Enlargement of Figure 3, showing c as a function of η_0 for various τ, including $\tau = \tau_{c3} \simeq -1.6547$, $\tau = \tau_{c4} \simeq -1.6504$ and $\tau = \tau_{c5} \simeq -1.6502$. The bounding curve on which $c = 1 + \tau$ is shown dashed.

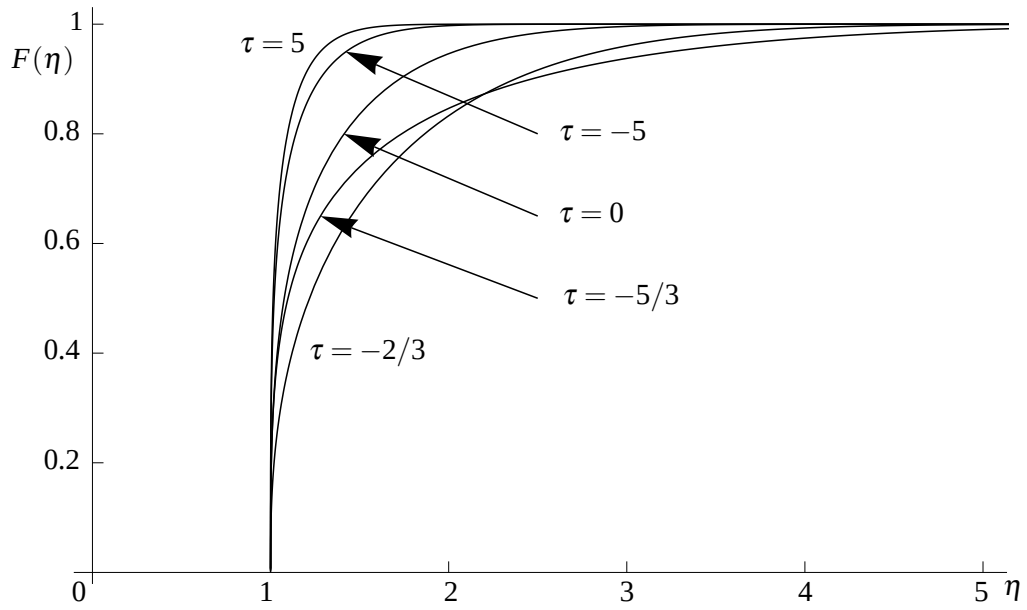

Figure 6: Cross-sectional profiles $F(\eta)$ for $\tau = 5$, 0, $-2/3$, $-5/3$ and -5, with $\eta_0 = 1$, for which $c \simeq 2.9611$, 0.4113, 0.04936, -0.5560 and -2.2820, respectively.

Figure 6 shows examples of cross-sectional profiles $F(\eta)$ for $\tau = 5$, 0, $-2/3$, $-5/3$ and -5 in the case $\eta_0 = 1$, for which it was found that $c \simeq 2.9611$, 0.4113, 0.04936, -0.5560 and -2.2820, respectively.

In all the cases that we have examined numerically, F increases monotonically with η, from $F = 0$ at $\eta = \eta_0$ to $F \to 1$ as $\eta \to \infty$ (consistent with the earlier discussion in Section 2.1). The curves for $\tau = 10$ and $\tau = -10$ in Figure 2 are nearly mirror-images of each other in the η_0 axis, reflecting the fact that for large enough $|\tau|$ the gravity-driven ingredient in the flow (associated with the term in $g\sin\alpha$ in (21)) is negligible in comparison with the shear-driven ingredient (associated with τ); for the same reason the cross-sectional profiles $F(\eta)$ for $\tau = 5$ and $\tau = -5$ in Figure 6 are somewhat similar.

3 CONCLUSIONS

We have obtained unsteady travelling-wave similarity solutions of the form (20) for an infinitely wide thin film of Newtonian fluid of nominal uniform thickness h_∞ flowing around a symmetric slender dry patch moving at constant velocity $c\mathbf{i}$ on an inclined planar substrate, the flow being driven by gravity and a constant shear stress τ at the free surface.

The dry patch has a parabolic shape, which may be concave up or concave down the substrate. If $\tau_\infty > 0$ (corresponding to a surface shear stress τ that either acts downwards or acts upwards but is sufficiently weak) then the dry patch moves down the substrate, whereas if $\tau_\infty < 0$ (corresponding to a sufficiently strong surface shear stress τ that acts upwards) then the dry patch moves up the substrate. It may be useful to note that by setting $\tau = 0$ in the governing equations, this problem will reduce to the problem of purely gravity-driven flow around the dry patch considered by [10].

In all cases investigated numerically the film thickness was found to increase monotonically away from the dry patch.

The parameter η_0 is not determined as part of the solution, so that (20) represents a one-parameter family of solutions; some additional criterion would be required to determine η_0.

The solutions obtained are valid for any value of h_∞, showing that for these solutions there is no critical thickness or critical flux below which a dry patch is stationary but above which it is *swept away* by the bulk flow.

The question of the stability of these dry-patch solutions is of interest, as is the question of the effect of surface tension on the flows; both of these are matters for future work.

REFERENCES

[1] A. B. Ponter, G. A. Davies, T. K. Ross and P. G. Thornley, "The influence of mass transfer on liquid film breakdown," Int. J. Heat Mass Transfer **10**, 349–359 (1967).

[2] D. E. Hartley and W. Murgatroyd, "Criteria for the break-up of thin liquid layers flowing isothermally over solid surfaces," Int. J. Heat Mass Transfer **7**, 1003–1015 (1964).

[3] E. Rio, A. Daerr and L. Limat, "Probing with a laser sheet the contact angle distribution along a contact line," J. Colloid Interface Sci. **269**, 164–170 (2004).

[4] E. Rio and L. Limat, "Wetting hysteresis of a dry patch left inside a flowing film," Phys. Fluids **18**, 032102 (2006).

[5] J. Sébilleau, L. Lebon and L. Limat, "Stability of a dry patch in a viscous flowing film," Eur. Phys. J. Special Topics **166**, 139–142 (2009).

[6] S. K. Wilson, B. R. Duffy and S. H. Davis, "On a slender dry patch in a liquid film draining under gravity down an inclined plane," Euro. J. Appl. Math. **12**, 233–252 (2001).

[7] T. Podgorski, J.-M. Flesselles and L. Limat, "Dry arches within flowing films," Phys. Fluids **11**, 845–852 (1999).

[8] T. Podgorski, J.-M. Flesselles and L. Limat, "Courbure de la frontière d'une zone sèche dans un film en écoulement (Curvature of a dry patch boundary in a flowing film)," C. R. Acad. Sci. Paris Sér. IV Physics **2**, 1361–1367 (2001).

[9] W. Murgatroyd, "The role of shear and form forces in the stability of a dry patch in two-phase film flow," Int. J. Heat Mass Transfer **8**, 297–301 (1965).

[10] Y. M. Yatim, B. R. Duffy and S. K. Wilson, "Travelling-wave similarity solutions for an unsteady gravity-driven dry patch," In *Progress in Industrial Mathematics at ECMI 2010*, Proceedings of the 16th European Conference on Mathematics for Industry (ECMI 2010), 26th–30th July 2010, Wuppertal, Germany, (eds. M. Günther, A. Bartel, M. Brunk, S. Schöps, M. Striebel), Springer 2012. pp. 441–448.